Thermal Atomic Layer Etching of Aluminum Oxide (Al2O3) Using Sequential Exposures of Niobium Pentafluoride (NbF5) and Carbon Tetrachloride (CCl4) : A Combined Experimental and Density Functional Theory Study of the Etch Mechanism

Sharma, Varun

American Chemical Society
2021-04-27

Sharma, V, Elliott, S D, Blomberg, T, Haukka, S, Givens, M E, Tuominen, M & Ritala, M 2021, 'Thermal Atomic Layer Etching of Aluminum Oxide (Al2O3) Using Sequential Exposures of Niobium Pentafluoride (NbF5) and Carbon Tetrachloride (CCl4) : A Combined Experimental and Density Functional Theory Study of the Etch Mechanism', Chemistry of Materials, vol. 33, no. 8, pp. 2883-2893. https://doi.org/10.1021/acs.chemmater.1c00142

http://hdl.handle.net/10138/343050
10.1021/acs.chemmater.1c00142

acceptedVersion

Thermal Atomic Layer Etching of Aluminum Oxide (Al_2O_3) using Sequential Exposures of Niobium Pentafluoride (NbF_5) and Carbon Tetrachloride (CCl_4): A Combined Experimental and Density Functional Theory Study of the Etch Mechanism

Varun Sharma,*,†,‡ Simon D. Elliott,¶ Tom Blomberg,§ Suvi Haukka,† Michael E. Givens,† Marko Tuominen,† and Mikko Ritala*,‡

†*ASM Microchemistry Oy, Pietari Kalmin katu 3 F2, Helsinki, Uusimaa 00560, Finland*

‡*Department of Chemistry, University of Helsinki, Helsinki, Uusimaa 00014, Finland*

¶*Schrödinger, 120 West 45th Street, New York, New York 10036-4041, USA*

§*Department of Chemistry and Materials Science, Aalto University, Espoo, Uusimaa 02150, Finland*

E-mail: varun.sharma@asm.com,varun.sharma@helsinki.fi; mikko.ritala@helsinki.fi

Abstract

Thermal atomic layer etching (ALEt) of amorphous Al_2O_3 was performed by alternate exposures of niobium pentafluoride (NbF_5) and carbon tetrachloride (CCl_4). The ALEt of Al_2O_3 is observed at temperatures from 380 to 460 °C. The etched thickness and etch rate were determined using spectroscopic ellipsometry (SE) and verified by X-ray reflectivity (XRR). The

maximum etch rate of about 1.4 Å/cycle and a linear increase of removed film thickness with number of etch cycles were obtained at a temperature of 460 °C. With the help of density functional theory (DFT) calculations, an etch mechanism is proposed where NbF_5 converts part of the Al_2O_3 surface into an AlF_3 or aluminum oxyfluoride layer, which upon reacting with CCl_4 is converted into volatile fluorine containing by-products, thus etching away the converted portion of the material. Consistent with this, a significant surface fluorine content of about 55 atomic % was revealed when the elemental depth profile analysis of a thick NbF_5-treated Al_2O_3 layer was performed by X-ray photoelectron spectroscopy (XPS). The surface morphology of the reference, pre and post-etch Al_2O_3 surfaces were analysed using atomic force microscopy (AFM) and bright field transmission electron microscopy (BF-TEM). Moreover, it is found that this process chemistry is able to etch Al_2O_3 selectively over silicon dioxide (SiO_2) and silicon nitride (Si_3N_4).

Introduction

In an era of emerging nano-technologies, the fabrication of sub-10 nm, complex and 3-D device structures demands unprecedented thickness control in the atomic-regime. Specific advances in semiconductor manufacturing techniques are therefore required[1–4] and several techniques are being actively developed, such as thermal atomic layer deposition (ALD),[5] plasma ALD, plasma-based atomic layer etching (ALE)[1,2,6] and the recently explored thermal atomic layer etching (ALEt).[7–9] Complementary to ALD, thermal ALEt is a technique that utilizes either partial or complete self-limiting sequential gas-solid reactions to allow removal of material from the surface with atomic-level precision.[7,10,11] Due to the self-limiting nature of at least one of the ALEt half-reactions, it can be preferred over plasma-based ALE for isotropic etching of material from non line-of-sight features.

Several thermal ALEt processes have been developed that employ a conversion-etch reaction mechanism.[12] During the conversion step, the surface is converted into a more reactive material, which during the etch step is exposed to a co-reactant and forms volatile products. In ALEt, the

conversion step can be forming an oxide,[13] fluoride[8–10] or other type of reactive surface that differs from the actual etch target. In the etch-step, ligands from the co-reactant molecules can undergo surface reactions such as ligand-exchange transmetalation,[7,8,11] fluorination[13] or chlorination[14,15] to form species that may leave the surface.

In most of the reported ALEt reactions, hydrogen fluoride (HF) is used as a fluorinating agent in either the conversion[7–11] or the etch step.[13] However, the use of HF can be restricted due to the safety concerns associated with its handling and storage. Moreover its corrosive nature can pose some compatibility issues with gas-feed as well as exhaust lines, pumps and other reactor parts especially when kept at elevated temperatures. Therefore alternatives to HF-based ALEt chemistries would prove beneficial. Several other highly reactive and toxic[16] fluorinating agents such as SF_4, XeF_2, F_2, CCl_2F_2 and $CHClF_2$ have been proposed.[17–20]

In this paper we explore a novel ALEt chemistry for etching amorphous Al_2O_3. It is proposed that NbF_5 can be used as a fluorinating agent, replacing HF. The CCl_4 is used to carry out the halide-exchange reactions with the fluorinated aluminum oxide surface in order to form volatile AlF_XCl_Y species. Moreover, CCl_4 is relatively more stable[21] than the trimethyl aluminum (TMA) used in the ALE literature,[8,9,11] which decomposes below 400°C..[22–24] Despite the NbF_5 being solid, it has sufficient vapor pressure (about 0.1 Torr at 45 °C[25]), forms volatile species upon fluorinating Al_2O_3 surface and thus leads to almost no surface contaminations. Moreover, it is relatively safer to handle, store, and compatible with the semiconductor vacuum processing equipments.

Experiment

Substrates and Process Gases

The target films deposited on p-type 200 mm silicon wafers that were used in the etch experiments are: thermally grown SiO_2 (TOx), high quality low pressure chemical vapor deposited (LPCVD) Si_3N_4 and ALD grown Al_2O_3. The SiO_2 and Si_3N_4 films were about 20 nm and 30 nm thick,

respectively. The Al_2O_3 films were deposited at 300 °C by the trimethylaluminum (TMA) and water (H_2O) ALD process.[26]

The fluorinating agent was 99.5% pure NbF_5 purchased from abcr GmbH, (Germany). The CCl_4 (anhydrous) was bought from Merck KGaA (Germany) and had purity $\geq$ 99.5%. The NbF_5 vessel was kept at 45 °C and the CCl_4 source vessel was operated at room temperature. CCl_4 has a vapor pressure of about 90 Torr at room temperature[27] and was therefore used in a vapor-draw, whereas the NbF_5 was used in vapor-push modes. Nitrogen (99.999%) was used as an inert purge gas. Both the purge gas flows as well as CCl_4 dose were controlled by needle valves.

Experimental Setup

The etch experiments were conducted on a Pulsar ® 2000 (P2000) cross-flow reactor manufactured by ASM International N.V. designed to process 200 mm silicon wafers. The P2000 chamber was operated at isothermal conditions to a maximum T_{etch} of 460 °C. Prior to any etching, all target substrates were kept in the vacuum chamber for 5 minutes in order to ensure stabilization of the wafer surface temperature. The chamber pressure was between 2 and 4 Torr.

Characterization Techniques

The thickness and optical constants of the films were evaluated using SE-800 spectroscopic ellipsometer from SENTECH Instruments GmbH, (Germany). An XRR used for confirming the removed thickness values, measuring the post-etched surface roughness and film densities was Xpert PRO MRD X-ray diffractometer from Malvern Panalytical Ltd (United Kingdom). For consistency, the exact center points of the wafers were chosen as measurement spots.

Elementary surface composition investigations were performed by X-ray photoelectron spectroscopy (XPS) and conducted on PHI Quantera SXM. Monochromatic Al-Kα (1486.6 eV/15 kV) X-rays with a take-off angle of 45°were used. The analysis chamber pressure was 3×10^{-6} Pa. In all the XPS depth profile measurements, the argon ion energy was set to 1 keV and the X-ray spot size was 100 µm. The pass energy of 140 eV was used. The detection limit of this particular tool

is about 0.1 - 0.5 atomic percent.

TEM imaging was performed by Evans Analytical Group (California, USA), on FEI Tecnai TF-20 FEG/TEM operated at 200 kV in a bright-field imaging mode. The TEM lamellas for imaging were prepared using focused ion beam (FIB) lift-out technique. The thicknesses of the TEM lamellas were around 100 nm. For preserving the contrast and structural integrity of the sample, a carbon coating was performed prior to the ion-milling.

Computational techniques

The chemical mechanism of the ALEt process was investigated using first principles density functional theory (DFT) as implemented in the Schrödinger *Materials Science* Suite.[28] Atomic-scale models of bulk materials, surfaces and gas-phase molecules were optimized under periodic boundary conditions with the Perdew-Burke-Ernzerhof (PBE) functional,[29] a plane wave basis to a wavefunction cut-off of 40 Ry, PBE ultrasoft pseudopotentials[30] and Monkhorst-Pack k-point sets[31] using the *Quantum ESPRESSO* code.[32,33] Total energies from DFT are used to calculate reaction energies ΔE for possible chemical transformations of these surfaces by the etchants during ALEt.

Since etching is likely to be driven by entropy (S), it is important to also determine reaction free energies (ΔG) that include the effect of temperature (T) and pressure of reactants (p_{react}) and products (p_{prod}), which for ideal gases at constant volume is given by: $\Delta G = \Delta E - T\Delta S - k_B T ln(\Pi p_{\text{prod}}^{\mu}/\Pi p_{\text{react}}^{\mu})$ where μ are stoichiometric coefficients.[34] For the etchants, we use p_{react}=0.1 Torr, approximating the experimental conditions, and assume equilibrium with product gases at p_{prod}=sp_{react} where the sticking coefficient s is an unknown precursor parameter that is typically in the range 10^{-2} to 10^{-4} for ALD precursors.[35] As explained in the Supplementary Information, the entropy terms at 100°C < T < 600°C and p_{react} or p_{prod} were derived from molecular vibrational analysis of the gas-phase reactant and product molecules at the PBE/LAV3D** level with the *Jaguar* code.[36]

The ($\bar{2}$ 0 1) surface of θ-Al_2O_3 was used as the periodic slab model for the alumina surface during ALEt. θ-Al_2O_3 was chosen because ions in this polymorph have a similar coordination

environment to those in amorphous as-deposited Al_2O_3.[37] The 2×1 expansion of a 3-layer ($\bar{2}$ 0 1) slab was selected as a representative model surface on the basis of its stability and level of corrugation when bare or fluorinated (see Supplementary Information).

As shown in Figure 1, half of the Al atoms on the bare surface are exposed (4-coordinate to O) and half are covered (6-coordinate). Fluorinated and chlorinated surfaces were generated by progressively replacing O with F or Cl in the topmost layer of the slab, always adding two halide monoanions for each oxide dianion removed so as to preserve stoichiometry and charge neutrality.

The maximum level of chlorination was determined to be 3Cl per 4-coordinate Al (12 Cl per 2×1 cell), which we designate as 100%-Cl coverage, since higher coverages led to the spontaneous desorption of $AlCl_3$ molecules during optimization. By contrast, fluorination up to 166%-F (20 F per 2×1 cell) was energetically favorable, albeit with substantial reorganization to give a surface resembling AlF_3 structural motifs. In this study we focus on interconversions between the 166%-F, 100%-F, 100%-Cl and 0% (i.e. bare alumina) surfaces depicted in Figure 1.

The aim of the DFT simulations is to map out the general form of the ALEt mechanism. Many reactions and by-products can be possible, and we seek here to distinguish which surface transformations are thermodynamically favourable as a function of process conditions. This can reveal the nature of the saturating surface after each precursor exposure during the ALEt cycle and hence account for the etch rate. However, ALEt is actually a non-equilibrium process, driven by kinetics and the irreversible removal of by-products from the surface into the gas flow. Computing the detailed sequence of surface adsorbates, intermediates, reaction pathways and associated kinetics with DFT would be a possible future step, but is beyond the current scope. It is worth remembering therefore, that a reaction computed here to be thermodynamically feasible (with $\Delta G < 0$ at a given T) may in fact face a high kinetic barrier and so not be observed on the experimental timescale. Nevertheless, in the absence of kinetic data, we assume that for a family of competing reactions, the kinetic barriers scale with reaction energies, and that therefore the most exoergic reaction is the most kinetically likely one.

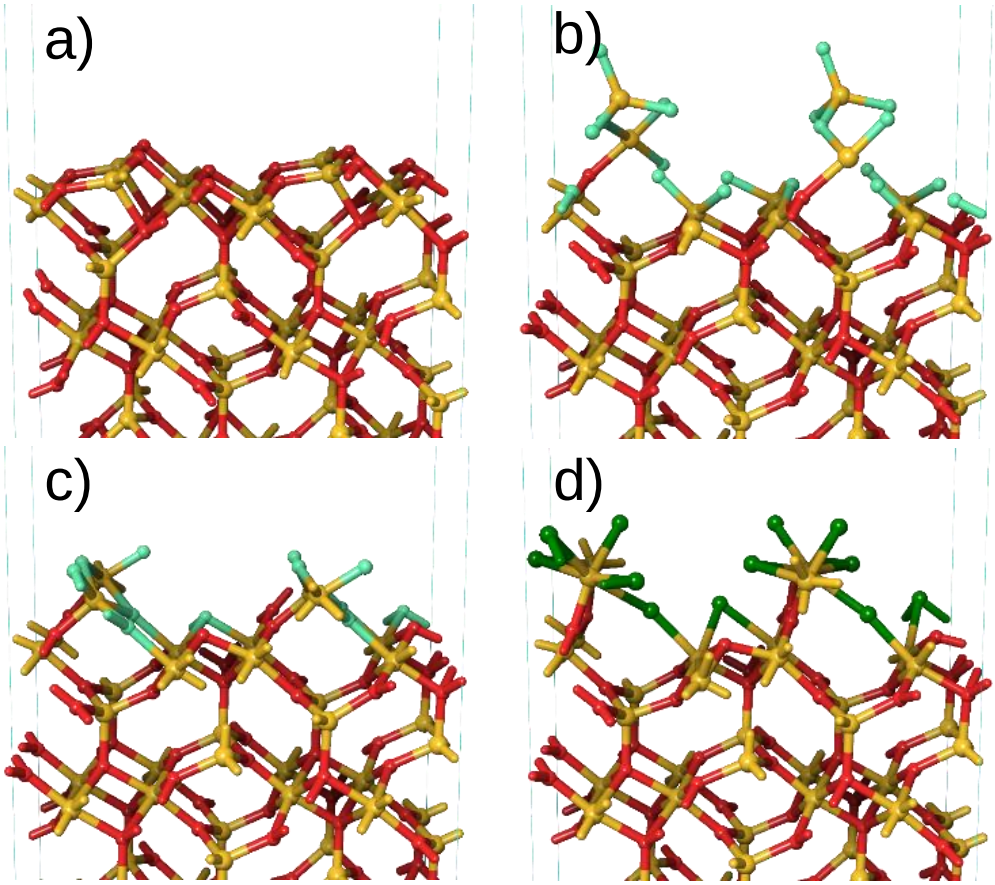

Figure 1: Structural models optimized with DFT for (a) bare Al_2O_3 surface with 0% halides, (b) surface covered with 166%-F, (c) 100%-F, (d) 100%-Cl. The colors are as follows: Al=yellow, O=red, F=light green, and Cl=dark green.

Results and Discussion

Etch-process Characterisation

Al_2O_3 is etched by utilizing sequential exposures of NbF_5 and CCl_4 precursors at elevated temperatures (380 - 460 °C). An inert gas purging was introduced after each exposure to remove the volatile by-products and excess of precursor molecules from the reaction chamber. The etch per cycle (EPC) was estimated by subtracting the post-etch thickness from initial thickness and dividing by the number of etch cycles. The Al_2O_3 film thickness values were reliably determined by spectroscopic ellipsometry and in some cases confirmed with the help of XRR and TEM images.

As shown in Figure 2, an increase in etch per cycle is observed with increasing NbF_5 pulse

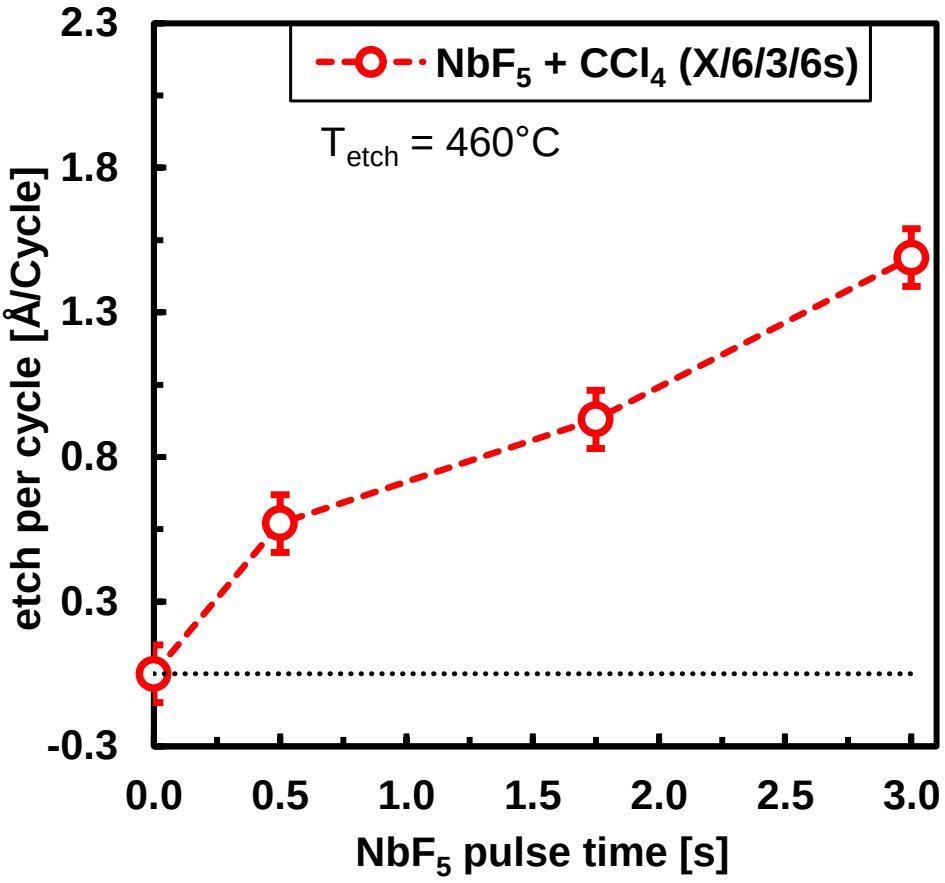

Figure 2: Change in etch per cycle vs NbF_5 pulse time at etch temperature of 460 °C. The CCl_4 pulse time was set to 3 s and in-between N_2 purges were 6 s, each.

time at an etch temperature (T_{etch}) of 460 °C. In the figure, NbF_5 pulse time is varied from 0 to 3 s while the CCl_4 pulse time is fixed to 3 s. For each data point plotted in the Figure 2, a total of 150 etch cycles were performed. In the absence of NbF_5, no Al_2O_3 etching was observed as confirmed by XRR, TEM and XPS. When the NbF_5 pulse time is increased to 0.5 s, an etch rate of about 0.5 Å per cycle is noticed. Further increase in the NbF_5 pulse time to 3 s provides an etch rate of about 1.4 Å/cycle. Longer NbF_5 pulse times were not tested. The figure shows that at T_{etch} of 460 °C, the EPC did not show strong self-limiting characteristic, but may still indicate a soft saturation behaviour. A non-saturative fluorination behaviour may affect the etch uniformity across the wafer especially in a cross-flow reactor. This non self-limiting behaviour can be explained by enhanced diffusion of fluoride ions at 460 °C. The thickness of converted layer may depend on factors such as surface temperature, partial pressure as well as flux of the precursor molecules,[9,11,38] reaction

time, adsorbate concentration, interaction between surface and diffusing adspecies, presence of defects, and accompanied by phase transitions etc.[39] Thus in thermal based ALE processes there may not exist an ALE window.

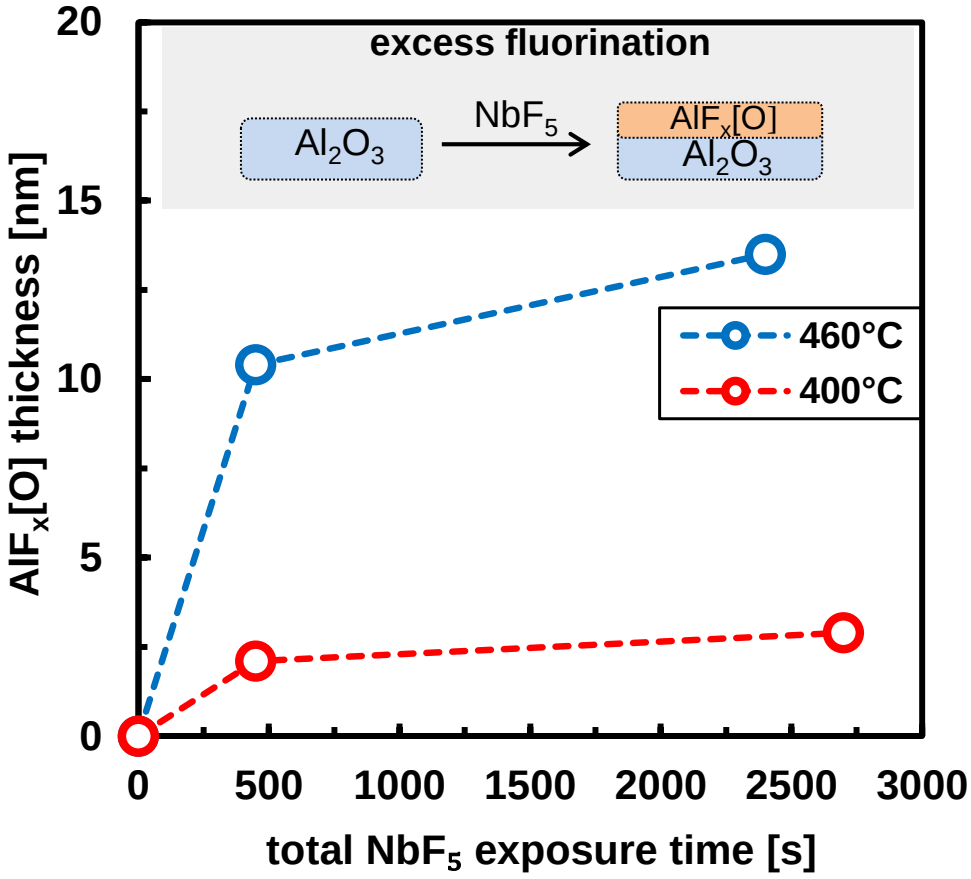

Figure 3: The $AlF_X[O]$ film thickness vs variation in total NbF_5 exposure time at 400 and 460 °C. The total NbF_5 exposure time is calculated from multiplying NbF_5 pulse time by total number of cycles. The NbF_5 pulse times of 4.5 s and 3 s were used at 400 and 460 °C, respectively. Each NbF_5 pulse separated by 6 s long N_2 purge step.

For studying the temperature-dependent kinetics of the fluorination step, excess fluorination was carried out by exposing the aluminum oxide surface to NbF_5 at 400 and 460 °C (Figure 3). At 400 °C, the excess fluorination was performed for 150 and 600 cycles of 4.5 s NbF_5 pulse times while 150 and 800 cycles of 3 s NbF_5 pulse times were used at 460 °C. After performing the excess fluorination step the thickness of the formed $AlF_X[O]$ layer was measured by ex-situ SE. About 11 nm and 14 nm thick fluorinated layers were obtained after 450 s and 2400 s of total NbF_5 exposure time respectively, at 460 °C. The formation of thick (>10 nm) $AlF_X[O]$ layers must be

due the prolonged fluorination step and the fluoride ions diffusing deeper into the aluminum oxide layer. The diffusion of fluoride is evident to be dependent on the temperature and thus may hint at existence of no ALE window. According to Morelock et al.,[40] aluminum trifluoride adopts the cubic form above 440 °C, which upon cooling changes to rhombohedral phase. The XRD analysis of about 11 nm AlF_X[O] layer revealed rhombohedral phase (see supplementary information S4) and is thus consistent with literature.[40–44] On the contrary, at 400 °C the thickness of the fluorinated layer stayed around 3 nm even after prolonged total NbF_5 exposure of 2700 s. Chao et al. showed the fluoride ions penetrating up to 2 nm thick aluminum oxide after treating fluorinated alumina at 400 °C,[45] and neutral/ion beams assisted fluorination lead to a thicker AlF_X[O] layer.[46] Moreover, up to 0.5 nm thick AlF_3 layer was obtained at lower temperature of 300 °C with HF as a fluorinating agent.[38] This temperature-dependent thickness of the converted fluorinated layer suggests that the conversion step is diffusion-limited.

The fluorination step produced a very hydrophilic surface with water contact angles $\leq 15°$, which is consistent with earlier reports from Roodenko et al..[19] The low water contact angle of the AlF_X[O] surface is attributed to high Lewis acidity of Al-F species, resulting in strong adsorption of H_2O molecules at under-coordinated aluminum sites.[19]

Figure 4 reveals the effect of variation in the CCl_4 pulse time on EPC at 460 °C. The NbF_5 pulse and N_2 purge lengths were set to 3 s and 6 s, respectively and the CCl_4 pulse time was changed from 0.5 to 3 s. The figure shows that an EPC around 1.1 Å is observed for CCl_4 pulse times between 0.5 s and 1.75 s. However, when 3 s CCl_4 pulse time is used an etch rate of 1.4 Å/cycle is noticed. This could indicate a partial self-limiting nature of the etching step, which could be due to limited AlF_X material available at the surface for CCl_4 to react with and volatilize. Moreover, Figures 3 and 4 together indicates a two-step ALEt mechanism of conversion followed by etching.

Figure 5 plots EPC values at various etch temperatures for the Al_2O_3 ALEt process by NbF_5 + CCl_4 (red curve). The figure also demonstrates that CCl_4 alone (blue curve) does not etch Al_2O_3 within the tested temperature range of 380 - 460 °C. The incapability of CCl_4 alone in etching Al_2O_3 is also confirmed by XRR and TEM images as seen below. However, at 380 °C the etch

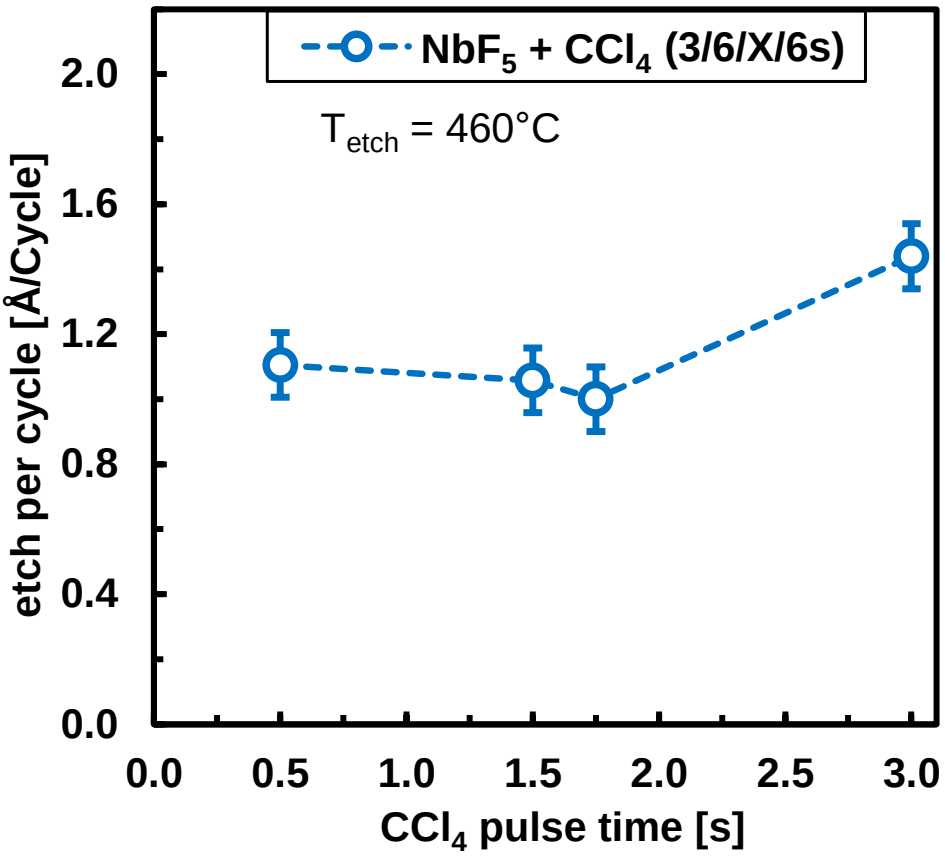

Figure 4: Effect of CCl_4 pulse time variation on etch per cycle at 460 °C. A total of 150 etch cycles were performed per data point.

rate of Al_2O_3 by the NbF_5 + CCl_4 ALEt process is comparatively low, at about 0.08 Å/cycle, and no significant etching was observed at temperatures < 380 °C. From the Figure 5, it can be seen that the EPC increases with the etch temperature and reaches an etch rate of 1.4 Å/cycle at 460 °C. The Figures 2 to 4 also corroborate the proposed ALEt mechanism, whereby NbF_5 is necessary to fluorinate the Al_2O_3 and the converted layer is etched by subsequent pulse of CCl_4. In most of the thermal ALE reports, the ALE window is not observed[9,11,12,38,47–50] and the EPC is dependent on the partial pressure[9,11,38] and temperature.[47,49,51] Similarly, it is evident from our findings that there exists no ALE window. However, a few ALE processes exhibits an ALE window such as ALE of HfO_2,[47] TiO_2[13] and TiN.[51]

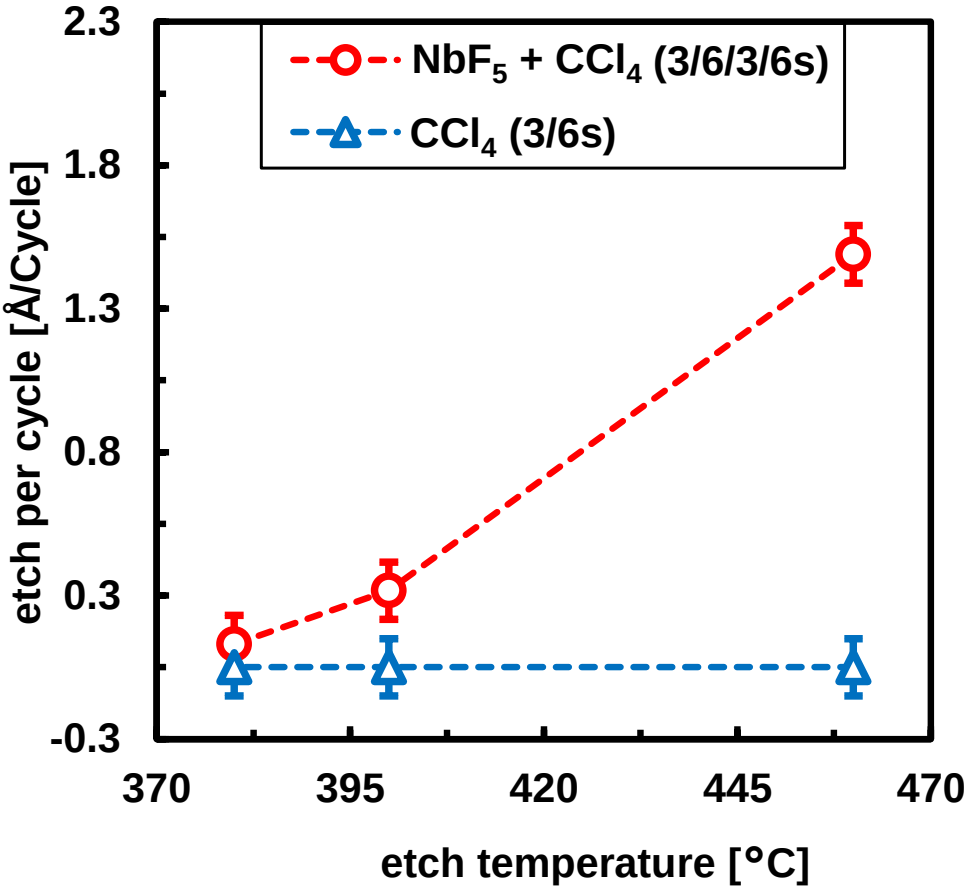

Figure 5: Change in etch per cycle with etch temperature for NbF_5 & CCl_4 cyclic etching process and compares to no-etching by CCl_4 only. Total 150 etch cycles were performed per data point. The EPC at etch temperatures below 380 °C stayed zero for both curves.

Selective Etching

In the thin film technology many applications may benefit from thermal ALEt processes that provide selective etching of Al_2O_3 over SiO_2 and Si_3N_4. Figure 6 shows that the NbF_5 + CCl_4 ALEt process is able to etch Al_2O_3 linearly with number of etch cycles at 460 °C. A linear fit of Al_2O_3 etched thickness with respect to etch cycles yields a constant etch rate of 0.11 nm/cycle when 0.5 s NbF_5 and 3 s CCl_4 pulse times are used. By contrast, under all the conditions tested here, no etching of SiO_2 and Si_3N_4 films was observed. In other words, between 380 and 460 °C, Al_2O_3 can be etched selectively over SiO_2 and Si_3N_4 by the NbF_5 + CCl_4 etch process.

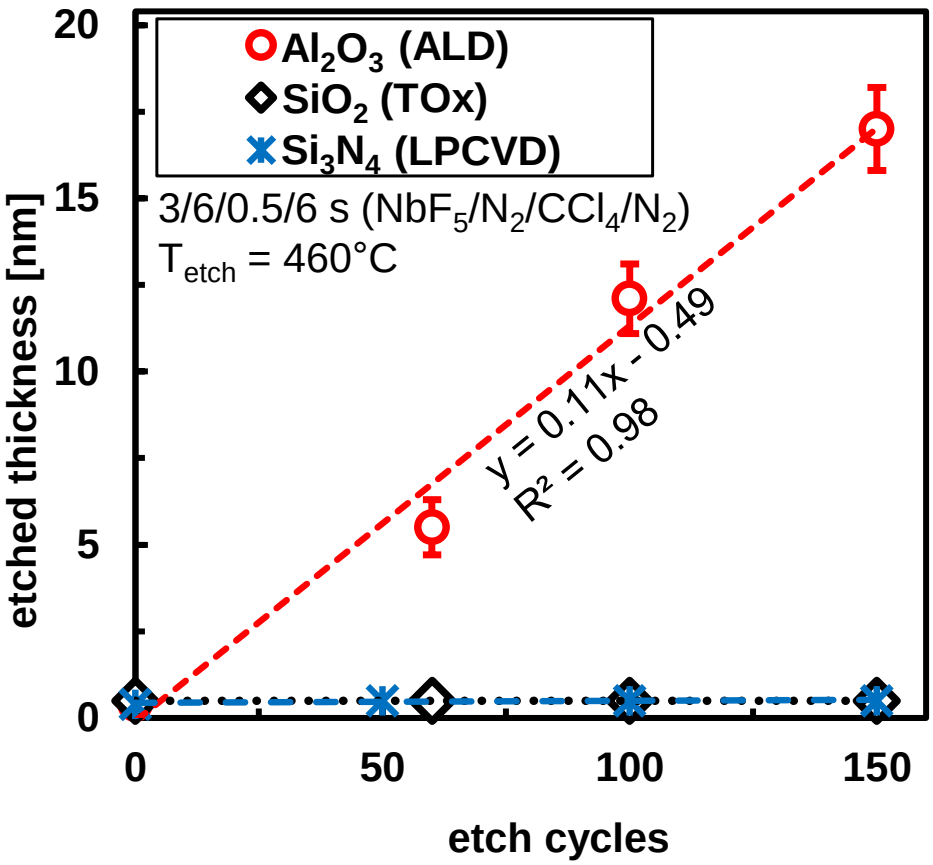

Figure 6: Etched thickness of Al_2O_3, SiO_2 and Si_3N_4 as a function of number of etch cycles at 460 °C. The NbF_5 and CCl_4 pulse times are 3 s and 0.5 s, respectively. The N_2 purge time was kept constant at 6 s.

Surface Characterization

XPS studies were conducted in order to understand the etch mechanism. An Al_2O_3 surface exposed to NbF_5 was the test subject. Figure 7 shows the XPS elemental depth profile analysis of the surface that has been fluorinated. The aluminum oxide surface was subjected to a total of 150 cycles of 3 s NbF_5 pulses with intermittent 6 s N_2 purges at 460 °C. Reasons for conducting the fluorination step under such extreme conditions were to ensure a significant as well as meaningful fluorine signal, to understand the fluorination step, and to deduce a reliable reaction mechanism. From the XPS depth profiling and SE measurements, the thickness of the $AlF_X[O]$ layer formed under these conditions was estimated to be around 11 nm.

After 15 s of sputtering, a very high fluorine content of about 55 atomic % (similar F content

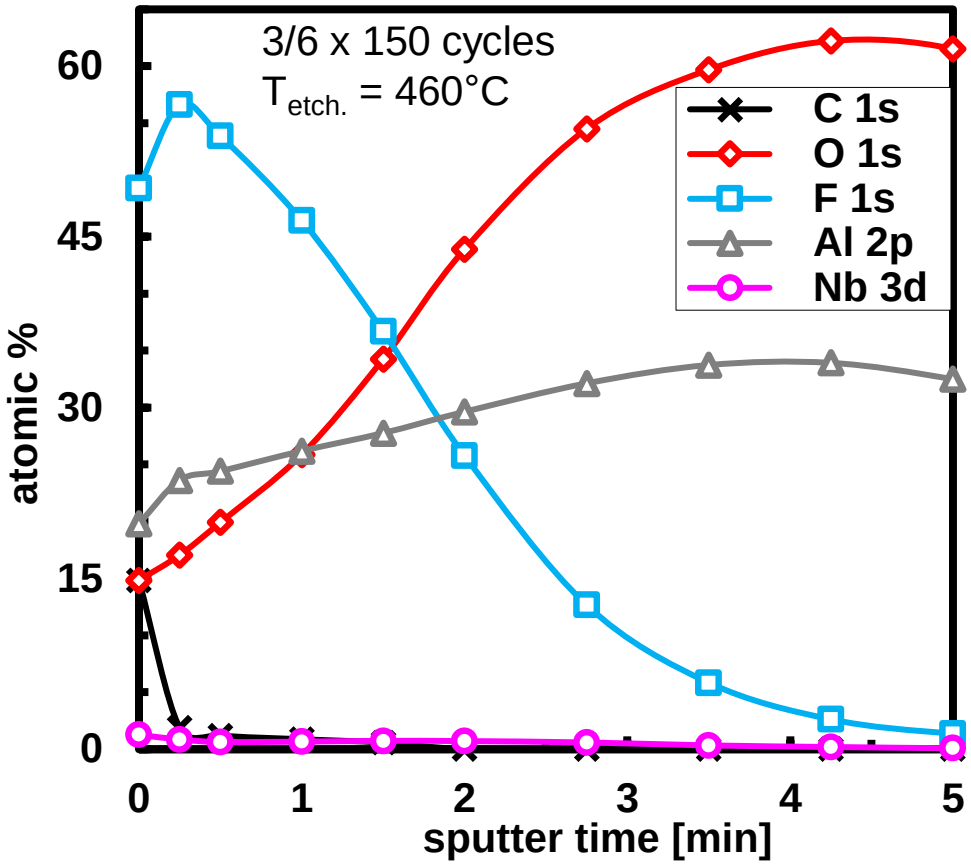

Figure 7: An XPS depth profile of Al_2O_3 exposed to NbF_5 for total of 450 s at 460 °C. The atomic percentage of elements found in the converted film is plotted with respect to sputter time.

was found by Kim et al.[52] after fluorinating Al_2O_3) and a decreased oxygen content of 17 atomic % (as compared to roughly 60 atomic % oxygen in Al_2O_3) is observed. The fluorine content gradually decreases with sputter time and may indicate a presence of gradient in the composition of the $AlF_X[O]$ layer. Furthermore, a very low niobium content of about 1 atomic %, decreased oxygen and high fluorine content support the proposed reaction mechanism in favour of reaction **R2** described below. This confirms that the NbF_5 molecules impart at least some fluoride ions to aluminum and forms volatile species with oxygen. Moreover, formation of about 11 nm thick $AlF_X[O]$ layer upon excess fluorination may explain the non self-limiting EPC curve in Figure 2.

Figure 8 reveals atomic percentages of several elements found on the Al_2O_3 surface as a function of sputtering time after removing about 18 nm of 56 nm Al_2O_3 film by the NbF_5 + CCl_4 ALEt process. A total of 150 ALEt cycles at 460 °C were performed with CCl_4 being the last pulse. The

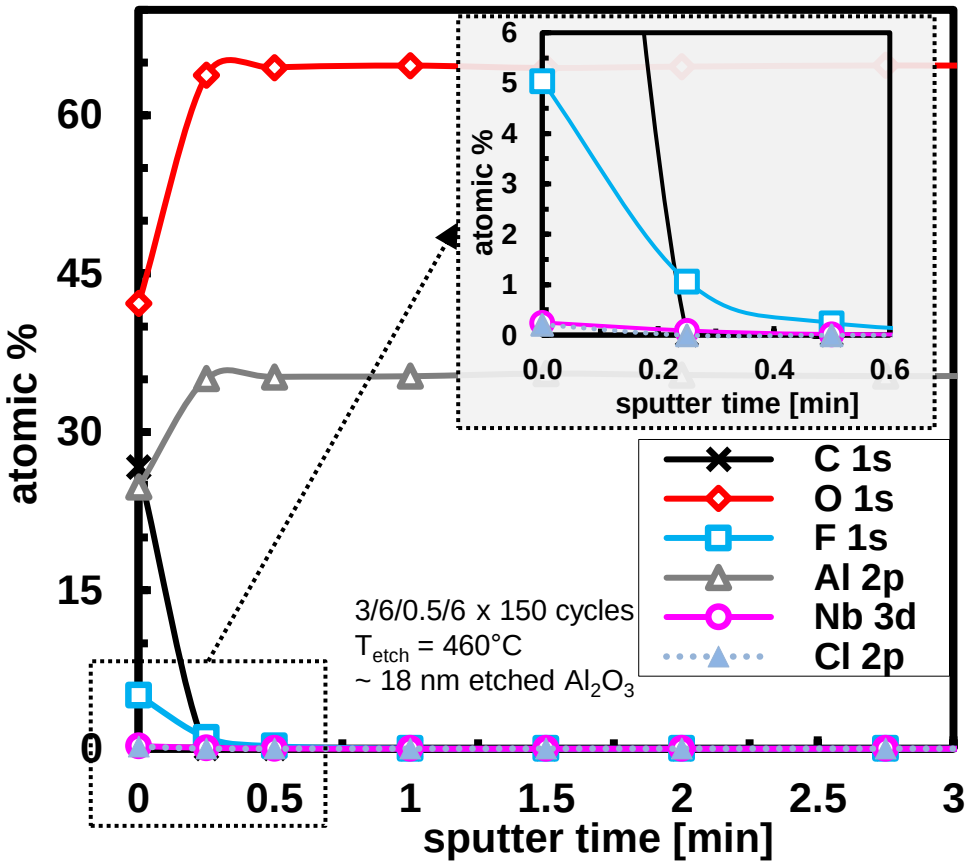

Figure 8: An XPS depth profile of remaining Al_2O_3 after removing about 18 nm film by NbF_5 and CCl_4 ALEt process. A zoomed picture at the top right corner focuses on Nb, F and Cl signals.

zoomed part of the figure depicts the fluorine content around 5 atomic % and very low amounts of niobium (< 0.3 atomic %) and chlorine (< 0.2 atomic %). The presence of surface fluorine may indicate that a CCl_4 pulse time longer than 0.5 s is necessary to either fully remove the converted layer or complete the halide-transmetalation reaction or it does not go to completion. From SE and XPS depth profiling the flourine-containing top layer is estimated to be around 1.2 nm thick.

In Figure 9, cross-sectional bright field transmission electron micrographs of Al_2O_3-coated silicon substrate are displayed. The thickness of a original Al_2O_3 film was 56 nm as revealed by SE and confirmed by XRR. Figure 9 a) shows the Al_2O_3 film that remained unetched after exposing it to 150 cycles of 3 s CCl_4 pulses. The figure also shows very smooth films devoid of significant surface defects. In Figure 9 b), it is shown that after exposing the Al_2O_3 film to 150 etch cycles of the NbF_5 + CCl_4 ALEt process, about 18 nm of the film is removed and the remaining

Al_2O_3 film appears to be rougher than the unetched film. In addition, AFM measurements (see SI) revealed a slight increase in the surface root mean squared (r.m.s. or R_a) roughness. This increase in surface roughness can be associated with the fluorination step and therefore can be due to either the variation in the diffusion depths or the reorganization of the near-surface region during diffusion-based fluorination. The etched surface does not appear to be crystalline.

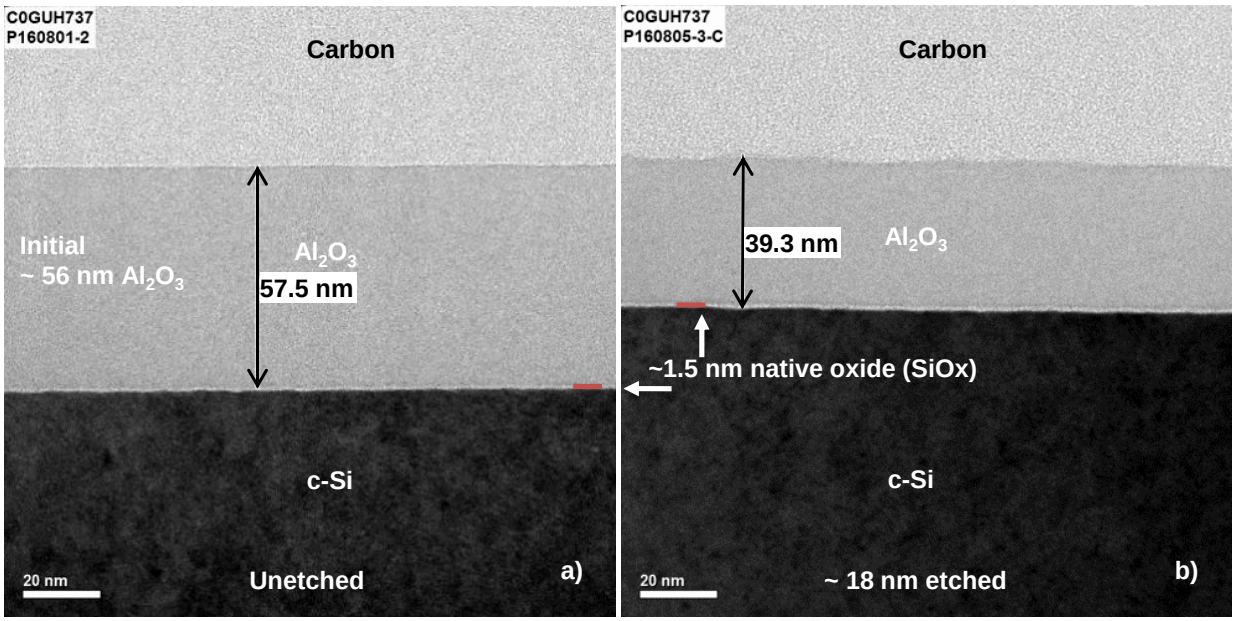

Figure 9: Cross-sectional bright field transmission electron microscope (BF-TEM) images of a) unetched 57.5 nm (includes 1.5 nm native silicon oxide) Al_2O_3 after exposing to 150 cycles of each 3 s long CCl_4 pulses, and b) after etching about 18 nm Al_2O_3 film by 150 cycles of NbF_5 + CCl_4 ALEt process. Initially about 56 nm Al_2O_3 was measured by SE (TEM not taken). The NbF_5 and CCl_4 pulse times were 3 s and 0.5 s, respectively. For both experiments, an etch temperature of 460 °C was used.

Computation of mechanism

Although the gaseous reactants undergo individual reaction steps when they adsorb to the surface during ALEt, along with bulk-surface diffusion, the net effect of an each cycle is the removal of bulk Al_2O_3 and regeneration of surface functionality. The most straightforward way to assess the viability of ALEt is therefore to compute the thermodynamics of bulk etching, which is presented next. Afterwards, DFT results for the thermodynamics of surface reactions are presented (more

details in the Supplementary Information.)

We first investigate whether it is thermodynamically favorable for either precursor alone to etch bulk alumina, transforming it into gas-phase products. NbF_5 can in principle remove both Al and O as follows:

$$\textbf{R1: } Al_2O_{3(s)} + 3NbF_{5(g)} \rightarrow 2AlF_{3(g)} + 3NbOF_{3(g)}$$

and for this reaction, periodic DFT yields ΔE=+140 kJ/mol-NbF_5 and ΔG^{300C}=-100 kJ/mol-NbF_5. The positive value of ΔE indicates a net cost in bond energies, while the negative value of ΔG reflects the entropy gain in volatilizing the solid. Bulk alumina may be more readily etched by the Cl source alone according to the reaction:

$$\textbf{R7: } Al_2O_{3(s)} + 3CCl_{4(g)} \rightarrow 2AlCl_{3(g)} + 3COCl_{2(g)}$$

which has DFT-computed energetics of ΔE=-18 kJ/mol-Al_2O_3 and ΔG^{300C}=-248 kJ/mol-Al_2O_3. (If the reaction would proceed to completion, CO_2 could be produced, but it seems more likely that $COCl_2$ would desorb first). However, no etching is observed experimentally with CCl_4 alone (Fig. 4), which suggests that kinetic barriers prevent this reaction taking place. Consistent with this, periodic DFT simulations show that the CCl_4 molecule resists adsorption to a bare alumina surface, probably because the molecule is non-polar. We therefore exclude these single-etchant reactions from the reaction equations below, and restrict our analysis to reactions that etch away either Al or O as volatile products, but not both simultaneously. Such reactions are the pre-requisite for a successful, self-limiting ALEt process.

The conversion of bulk alumina into solid aluminum fluoride according to:

$$\textbf{R2: } Al_2O_{3(s)} + 3NbF_{5(g)} \rightarrow 2AlF_{3(s)} + 3NbOF_{3(g)}$$

is computed to show ΔE=-24 kJ/mol-NbF_5 and $\Delta G^{300\ ^{\circ}C}$=-58 kJ/mol-$NbF_5$ (Table 1). Although

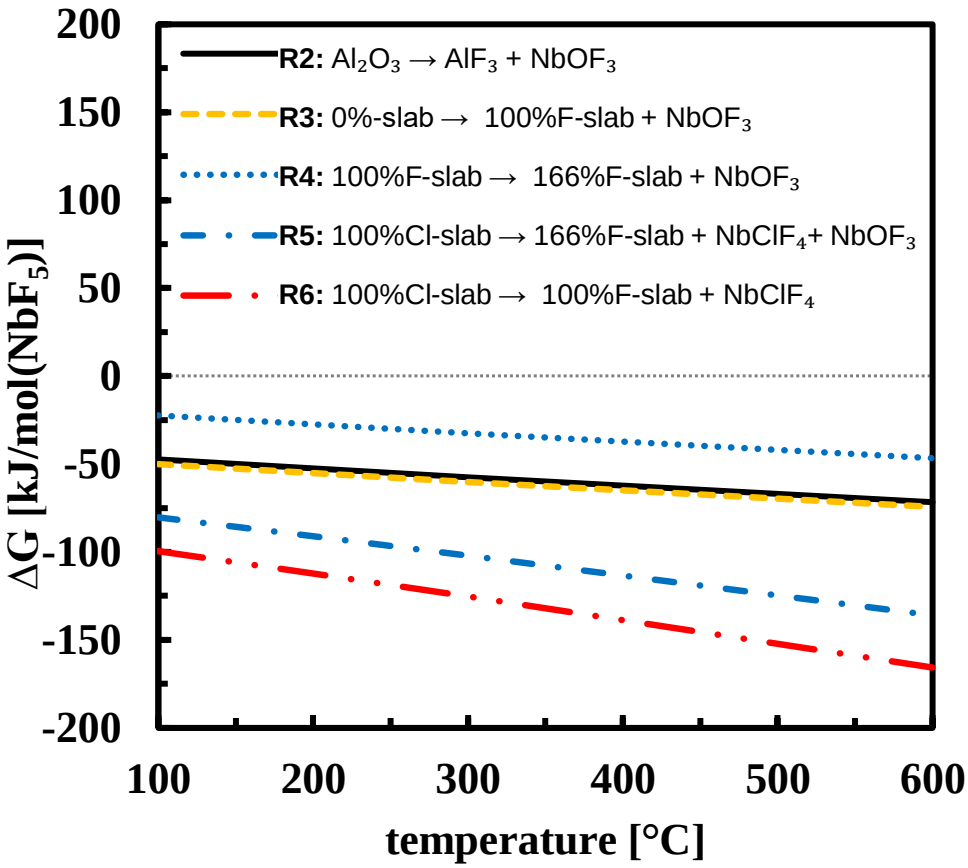

Figure 10: Change in the Gibbs free energy with temperature for various fluorination ALEt-half reactions.

labelled as 'conversion' in the ALEt literature, this reaction necessarily involves the etching of oxygen, as one oxide dianion is exchanged with two fluoride monoanions. The thermodynamics of conversion of the bare alumina surface into a 100%-fluorinated surface is found to be similar in terms of energetics to that of the bulk (**R3:** ΔE=-27 kJ/mol-NbF_5 and $\Delta G^{300\ ^\circ C}$=-60 kJ/mol-NbF_5). Further fluorination of the surface is slightly less favorable (e.g. **R4:** ΔE=+0.8 kJ/mol-NbF_5 and $\Delta G^{300\ ^\circ C}$=-33 kJ/mol-NbF_5 for 100%F to 166%F), but still exoergic, indicating that surface conversion does not self-limit. As shown in Figure 10, there is little variation with temperature in these free energies of fluorination of the bulk and surface by NbF_5.

We conclude that continuous conversion of alumina into aluminum fluoride is moderately exoergic under the experimental conditions, but again, the extent to which such conversion actually takes place depends on the kinetics of individual steps that bring NbF_5 and alumina into contact.

We suggest that this is likely to be dictated by the kinetics of diffusion across the Al_2O_3-AlF_3 interface. The NbF_5 pulse therefore produces a surface layer and possibly also sub-surface layers that are fluorinated and is experimentally verified in the Figures 3 and 7.

We now examine the potential reactions of such fluorinated surfaces (considering the sample surfaces 100%F and 166%F) with gas-phase CCl_4 in the next phase of the ALEt cycle. The computations show that the most energetically favorable products are $CFCl_3$ and $AlCl_3$ and the resulting thermodynamics are given in Table 1 and Figure 11.

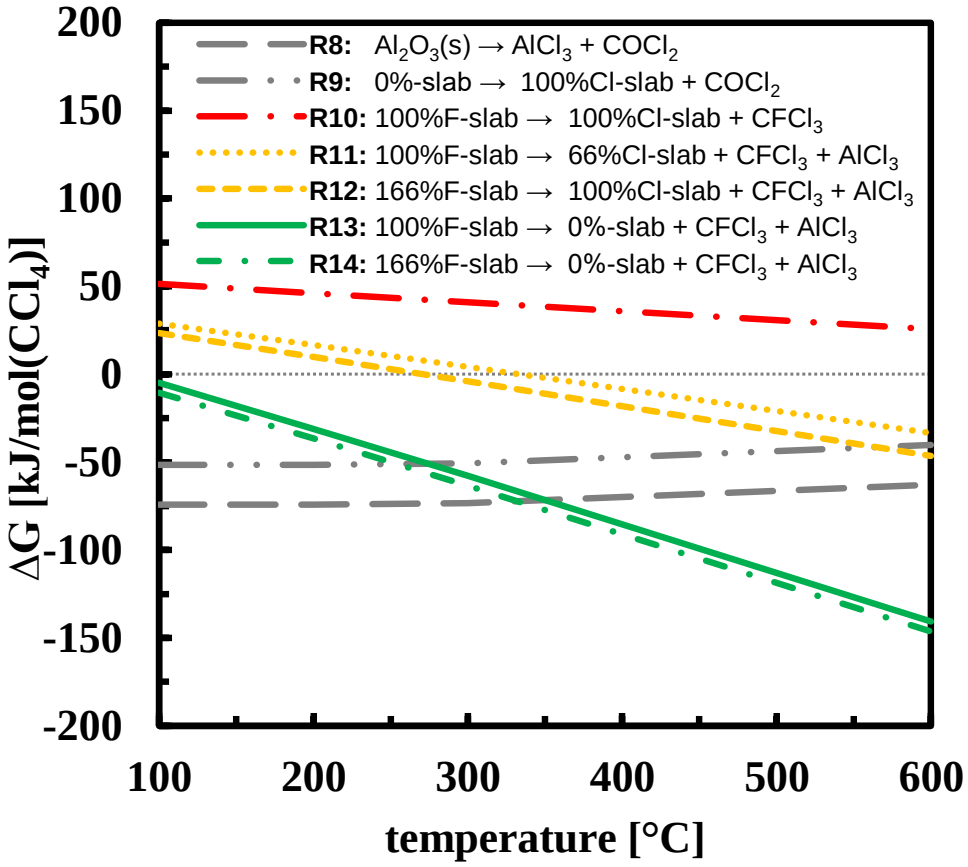

Figure 11: Change in the Gibbs free energy with temperature for possible chlorination or halide-exchange reactions.

$CFCl_3$ is the likely product of halide-exchange between the CCl_4 reagent and the fluorinated surface. The simplest such reaction produces a chlorinated surface with the same coverage:

$$\textbf{R10: } 100\%\text{F-slab} + 12CCl_{4(g)} \rightarrow 100\%\text{Cl-slab} + 12CFCl_{3(g)}$$

which is computed to be endoergic across a wide temperature range (ΔG^{300C}=+41 kJ/mol-CCl_4). The reaction becomes more favorable if Al is also etched away as $AlCl_3$. For instance, ΔG^{300C}=+4.3 kJ/mol-CCl_4 for partial etching:

R11: $100\%\text{F-slab} + 12CCl_{4(g)} + 2/3Al_2O_{3(s)} \rightarrow 66\%\text{Cl-slab} + 12CFCl_{3(g)} + 4/3AlCl_{3(g)}$

and ΔG^{300C}=-58 kJ/mol-CCl_4 for complete etching to a bare surface:

R13: $100\%\text{F-slab} + 12CCl_{4(g)} + 2Al_2O_{3(s)} \rightarrow 0\%\text{-slab} + 12CFCl_{3(g)} + 4AlCl_{3(g)}$.

Table 1: Reaction thermodynamics computed with DFT for potential half-reactions in the NbF_5 pulse (reactions R1-R6) and CCl_4 pulse (R7-R14), as well as the overall ALEt cycle (R15). Bulk solid is labelled (s), gas-phase molecules (g) and coverage is indicated as a percentage for surface slabs.

R. No.	Reaction	ΔE	$\Delta G^{100\,°C}$	$\Delta G^{200\,°C}$	$\Delta G^{300\,°C}$	$\Delta G^{600\,°C}$	units
R1	$Al_2O_{3(s)} + 3NbF_{5(g)} \rightarrow 2AlF_{3(g)} + 3NbOF_{3(g)}$	139.9	-10.2	-54.6	-100.1	-241.4	$\frac{kJ}{mol(NbF_5)}$
R2	$Al_2O_{3(s)} + 3NbF_{5(g)} \rightarrow 2AlF_{3(s)} + 3NbOF_{3(g)}$	-24.1	-47.4	-52.5	-57.5	-71.7	$\frac{kJ}{mol(NbF_5)}$
R3	$0\%\text{-slab} + 6NbF_{5(g)} \rightarrow 100\%\text{F-slab} + 6NbOF_{3(g)}$	-26.8	-50.1	-55.3	-60.3	-74.5	$\frac{kJ}{mol(NbF_5)}$
R4	$100\%\text{-slab} + 4NbF_{5(g)} \rightarrow 166\%\text{F-slab} + 4NbOF_{3(g)}$	0.8	-22.4	-27.6	-32.6	-46.8	$\frac{kJ}{mol(NbF_5)}$
R5	$100\%\text{Cl-slab} + 16NbF_{5(s)} \rightarrow 166\%\text{F-slab} + 12NbClF_{4(g)} + 4NbOF_{3(g)}$	-44.9	-80.4	-91.1	-102.1	-136.0	$\frac{kJ}{mol(NbF_5)}$
R6	$100\%\text{Cl-slab} + 12NbF_{5(s)} \rightarrow 100\%\text{F-slab} + 12NbClF_{4(g)}$	-60.1	-99.7	-112.3	-125.3	-165.7	$\frac{kJ}{mol(NbF_5)}$
R7	$Al_2O_{3(s)} + 3CCl_{4(g)} \rightarrow 2AlCl_{3(g)} + 3COCl_{2(g)}$	-17.7	-164.1	-206.0	-248.4	-372.9	$\frac{kJ}{mol(CCl_4)}$
R8	$Al_2O_{3(s)} + 3CCl_{4(g)} \rightarrow 2AlCl_{3(s)} + 3COCl_{2(g)}$	-62.8	-74.2	-74.1	-73.4	-62.8	$\frac{kJ}{mol(CCl_4)}$
R9	$0\%\text{-slab} + 6CCl_{4(g)} \rightarrow 100\%\text{Cl-slab} + 6COCl_{2(g)}$	-40.1	-51.6	-51.5	-50.7	-40.2	$\frac{kJ}{mol(CCl_4)}$
R10	$100\%\text{F-slab} + 12CCl_{4(g)} \rightarrow 100\%\text{Cl-slab} + 12CFCl_{3(g)}$	72.5	51.4	46.2	41.0	25.7	$\frac{kJ}{mol(CCl_4)}$
R11	$100\%\text{F-slab} + 12CCl_{4(g)} + (2/3)Al_2O_{3(s)} \rightarrow 66\%\text{Cl-slab} + 12CFCl_{3(g)} + (4/3)AlCl_{3(g)}$	72.5	28.9	16.7	4.3	-33.5	$\frac{kJ}{mol(CCl_4)}$
R12	$166\%\text{F-slab} + 20CCl_{4(g)} + (4/3)Al_2O_{3(s)} \rightarrow 100\%\text{Cl-slab} + 20CFCl_{3(g)} + (8/3)AlCl_{3(g)}$	71.5	23.3	9.7	-4.1	-46.4	$\frac{kJ}{mol(CCl_4)}$
R13	$100\%\text{F-slab} + 12CCl_{4(g)} + 2Al_2O_{3(s)} \rightarrow 0\%\text{-slab} + 12CFCl_{3(g)} + 4AlCl_{3(g)}$	83.7	-4.9	-31.1	-57.9	-140.6	$\frac{kJ}{mol(CCl_4)}$
R14	$166\%\text{F-slab} + 20CCl_{4(g)} + (10/3)Al_2O_{3(s)} \rightarrow 0\%\text{-slab} + 20CFCl_{3(g)} + (20/3)AlCl_{3(g)}$	78.2	-10.4	-36.6	-63.4	-146.2	$\frac{kJ}{mol(CCl_4)}$
R15	$Al_2O_{3(s)} + 3NbF_{5(g)} + 6CCl_{4(g)} \rightarrow 2AlCl_{3(g)} + 3NbOF_{3(g)} + 6CFCl_{3(g)})$	421.8	-62.6	-194.2	-329.1	-747.6	$\frac{kJ}{mol(Al_2O_3)}$

Similar results for the 166%F surface are displayed in Figure 11. As expected, these etch reactions are driven by entropy and thus become more favored at high temperature. We can not confidently state the exact temperature above which a given reaction becomes exoergic, since this is affected by the pressure correction and thus by the arbitrary choice of sticking coefficient *s*. Nevertheless, Figure 11 allows us to conclude that it is thermodynamically favored for CCl_4 to entirely etch away the aluminum fluoride layer and reveal bare alumina (0% surface).

Since CCl_4 may in principle etch bulk alumina (reaction **R7**), we need to consider whether the bare alumina surface is reactive with this precursor. Converting the bare surface to a 100%-chlorinated surface is found to be exoergic, with ΔE=-40 kJ/mol-CCl_4 and ΔG^{300C}=-51 kJ/mol-CCl_4 (reaction **R9**) following a similar trend to the conversion of bulk alumina to bulk aluminium chloride (reaction **R8**). However, as noted above, the experimental result of no etching by CCl_4 alone indicates that this reaction pathway is not accessible. A bare alumina surface is therefore the thermodynamically favored outcome of the CCl_4 pulse.

In case fluorinated or chlorinated portions of the surface persist into the NbF_5 pulse of the next ALEt cycle, we include exemplary reactions of 100%F and 100%Cl surfaces with NbF_5 in Fig. 10 (reactions **R4**, **R5** and **R6**). In this case, halide-exchange to $NbClF_4$ is the most favorable reaction, but addition of F and removal of O is also exoergic across the entire temperature range. Therefore, these reactions also lead to a fluorinated surface as the outcome of the NbF_5 pulse.

Having identified the saturated surfaces at the end of each precursor pulse, we are now able to combine half-reactions (**R3**+**R13** or **R4**+**R14**) into the overall ALEt reaction:

$$\textbf{R15:}\ Al_2O_{3(s)} + 3NbF_{5(g)} + 6CCl_{4(g)} \rightarrow 2AlCl_{3(g)} + 3NbOF_{3(g)} + 6CFCl_{3(g)}$$

The overall energies per ALEt cycle computed with DFT are ΔE=+421 kJ/mol-Al_2O_3 and ΔG^{300C}=-329 kJ/mol-Al_2O_3.

Consistent with the data in Figure 2, the etch rate per cycle (EPC) in this mechanism depends on the level of conversion that is achieved in the NbF_5 pulse. 100%F means the etching of $2Al_2O_3$/cycle in the 2×1 slab. Dividing by the cross-sectional area of the slab (84.5 $Å^2$) and multi-

plying by the molar volume of θ-alumina (48.5 $Å^3/Al_2O_3$) yields a theoretical EPC of 1.2 Å/cycle for this F-coverage. Converting a greater proportion of the surface zone to AlF_3 means a higher EPC - for example 166%F means etching 3.3 (Al_2O_3)/cycle per slab and an EPC of 1.9 Å/cycle.

Proposed Reaction Mechanism

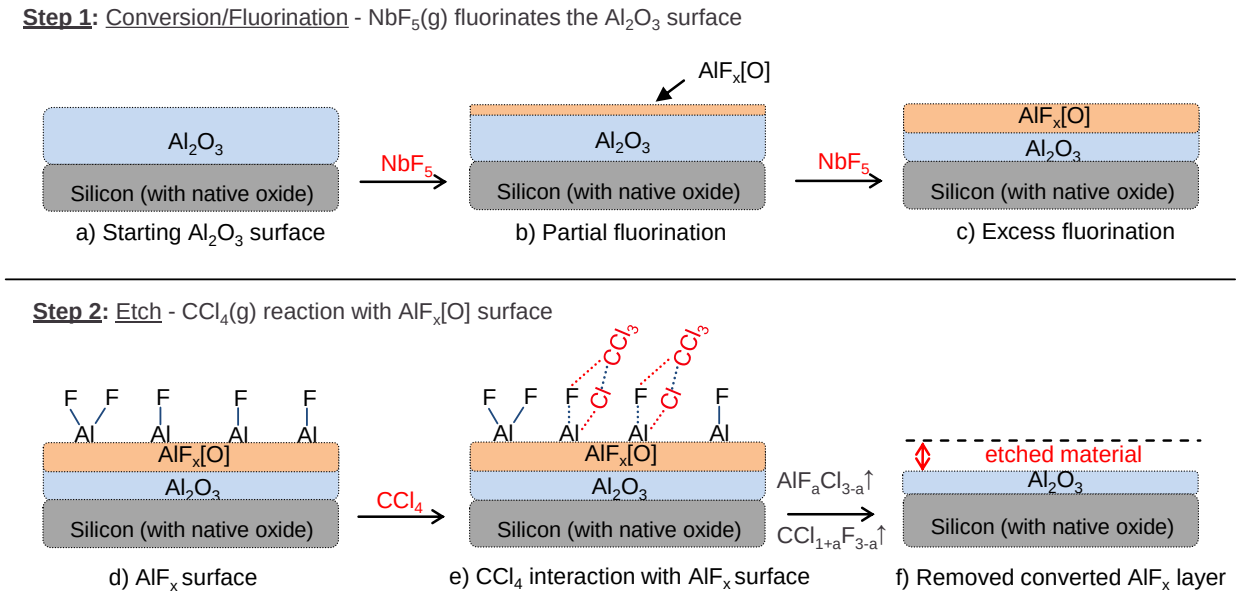

Figure 12: The proposed ALEt mechanism consists of a conversion step followed by an etch step: a) starting Al_2O_3 surface, b) after partial fluorination by NbF_5, c) upon excess NbF_5 exposure a thick $AlF_X[O]$ is formed, d) $AlF_X[O]$ surface with Al-F bonds, f) possible halide-exchange interaction between CCl_4 and $AlF_X[O]$ surface, g) removed converted $AlF_X[O]$ layer and revealed underlying Al_2O_3 surface.

Many reported thermal ALEt reactions undergo a two-step, conversion-etch mechanism,[7–11,13] with the conversion (or fluorination) step followed by an etch step. The experimental findings in this report also suggest a two-step etch mechanism.

The first step of the proposed reaction mechanism shown in Figure 12 is the conversion step. Figure 12 a), depicts the initial Al_2O_3 film on the silicon substrate and the Figure 12 b) shows the fluorinated Al_2O_3 layer after exposing to the NbF_5. As evident from the figures 3 and 7, the NbF_5 is believed to act like a fluorinating agent similar to HF[7] or WF_6[13] and converts the Al_2O_3 surface into $AlF_X[O]$. The experimental findings suggest that the fluorination is not self-

limiting and therefore with excessive fluorination a thicker $AlF_X[O]$ layer is formed, as depicted in Figure 12 c).

From the DFT calculations for gas-bulk (**R1, R2**) as well as gas-surface reactions (**R3-R5**), it is proposed that niobium most likely forms the volatile $NbOF_3$ species. The existence of gaseous $NbOF_3$ has been previously reported and its volatility has been studied.[53–56] The reaction $NbOF_{3(s)} \longrightarrow NbOF_{3(g)}$ is favorable ($\Delta G < 0$) above 140 °C.[25] Moreover, thermogravimetric analysis of $NbOF_3$ showed mass loss above 80 °C.[25]

During this conversion-step, the oxygen from Al_2O_3 layer is also removed at least partially if not completely and therefore the fluorinated layer is labelled as $AlF_X[O]$. Figure 12 d) depicts an outcome of the excess fluorination step and is supported by Figures 3 and 7.

In the second step, the $AlF_X[O]$ layer can be etched as shown in Figure 12 from d) to f). The etch step involves halide-exchange transmetalation to form volatile by-products such as AlF_aCl_{3-a} and $CCl_{1+a}F_{3-a}$, where $0 \leq a \leq 2$. The DFT computations reveal $AlCl_3$ and $CFCl_3$ as being the most favorable etch products from the various chlorination half reactions **R10-R14**. In this fashion an etching of Al_2O_3 can be achieved by alternating exposures of NbF_5 and CCl_4, which may follow the described conversion-etch mechanism by overall reaction **R15**.

Discussion of etch rate

According to the overall etch reaction **R15**, the theoretical EPC of 1.2 Å/cycle for 100%F-slab coverage is evaluated. For prolonged fluorination as per reactions **R4** and **R5**, where 166%F-slab is used an EPC of 1.7 Å/cycle is obtained. An EPC of 1.4 Å/cycle is recorded for 3 s NbF_5 and CCl_4 pulse lengths (as shown in Figure 2), which is therefore consistent with a coverage of 120%F during etching by **R15**. Moreover, both the experiment and the DFT calculations indicate that the EPC is not self-limiting for NbF_5 pulse time variation and strongly depends on the fluorination step.

Another parameter that largely impacts the EPC is the etch temperature. Higher EPC values are observed at higher temperatures (≥380°C). At temperatures below 380°C no etching was ob-

served. However, DFT thermodynamic calculations did not show any evidence for this behaviour. Therefore, this temperature dependence probably reflects the kinetics of diffusion and structural reorganization at the Al_2O_3-AlF_3 interface. Based on our examination of the DFT-computed structures, it may be that atoms near the interface have to reorganize so that aluminum takes a low coordination number (i.e. 4 rather than 6) as the pre-requisite for the fluoride to form, and hence for the etching to take place.

Summary

Thermal atomic layer etching (ALEt) of amorphous Al_2O_3 is demonstrated using cyclic exposures of NbF_5 and CCl_4 etchants. The Al_2O_3 ALEt is found to follow a two-step etch mechanism. In the first step, NbF_5 converts part of the Al_2O_3 layer into $AlF_X[O]$, or more evidently AlF_3, which is described as a conversion or fluorination step. The most likely volatile by-product is found to be $NbOF_3$. In the second step, the chlorine atoms from CCl_4 undergo halide-exchange with the converted $AlF_X[O]$ surface. As a result of such an interaction various volatile by-products such as AlF_2Cl, $AlFCl_2$, $AlCl_3$ and several chlorofluorocarbon molecules can be produced. Of these, $AlCl_3$ and $CFCl_3$ are found by DFT to be the most favorable, which leads to the overall etching reaction:

$$Al_2O_{3(s)} + 3NbF_{5(g)} + 6CCl_{4(g)} \rightarrow 2AlCl_{3(g)} + 3NbOF_{3(g)} + 6CFCl_{3(g)}.$$

Similar reactions can be written for the other possible by-products.

In this manner, the converted $AlF_X[O]$ layer is volatilized from the surface by CCl_4 and hence the desired etching takes place. The feasibility of the proposed reaction mechanism was confirmed with thermodynamic calculations based on DFT. In addition, XPS and XRD analyses confirmed the formation as well as removal of the fluorinated $AlF_X[O]$ layer.

The dependence of etch rate per cycle on NbF_5 pulse time shows soft self-limiting characteristics, which can be due to slow kinetics, diffusion-limited gas-solid reaction, high residence time of

NbF_5, low concentration or partial pressure of NbF_5 or slow sublimation of volatile $NbOF_3$ surface species. The CCl_4 reaction is found to be more self-limiting than that of NbF_5.

Aluminum oxide ALEt is observed between 380 and 460 °C. From its onset (removing just 0.08 Å/cycle at 380 °C), the etch rate tends to increase with etch temperature. We tentatively link this temperature-dependence to the kinetics of diffusion across the oxide-fluoride interface. The linear removal of Al_2O_3 with cycles is observed with an etch rate of about 1.1 Å/cycle at 460 °C. An etch rate of about 1.4 Å/cycle is measured when the exposure time for each precursor is set to 3 s, separated by 6 s N_2 purges. This etch rate is consistent with fluorination that extends partly into the subsurface layer. As revealed by TEM analysis, the surface of the post-etch Al_2O_3 film was rougher than the unetched film, again pointing to diffusion at the interface.

It is proposed that the thermal NbF_5 + CCl_4 ALEt process reported here could etch other metal oxides in a similar two-step etch mechanism with selectivity against SiO_2 and Si_3N_4.

Acknowledgment

The authors thank Mr. Bernd Böck from Tascon GmbH (Münster, Germany) for XPS depth profile analysis of the Al_2O_3 films. We acknowledge the support from Eurofins EAG Materials Science, LLC (California, USA) for the TEM analysis and understanding the data associated with it.

Supporting Information Available

The attached supplementary information includes the details on DFT calculations, GIXRD analysis of the aluminum fluoride and surface morphology by atomic force microscopy. Moreover, the attached "theta-Al_2O_3-structures.zip" folder includes the computed bare slabs in crystallographic information file (.cif) format for our readers.

References

(1) Kanarik, K. J.; Lill, T.; Hudson, E. A.; Sriraman, S.; Tan, S.; Marks, J.; Vahedi, V.; Gottscho, R. A. Overview of atomic layer etching in the semiconductor industry. *Journal of Vacuum Science & Technology A* **2015**, *33*, 020802.

(2) Oehrlein, G.; Metzler, D.; Li, C. Atomic Layer Etching at the Tipping Point: An Overview. *ECS Journal of Solid State Science and Technology* **2015**, *4*, N5041–N5053.

(3) Kuhn, K. J.; Liu, M. Y.; Kennel, H. Technology options for 22nm and beyond. *International Workshop on Junction Technology Extended Abstracts, Shanghai, China* **2010**, 1–6.

(4) Kuhn, K. J. et al. The ultimate CMOS device and beyond. *International Electron Devices Meeting, San Francisco, CA, USA* **2012**, 8.1.1–8.1.4.

(5) Haukka, S. ALD Technology - Present and Future Challenges. *ECS Transactions* **2007**, *3 (15)*, 15–26.

(6) Marchack, N.; Chang, J. P. Perspectives in nanoscale plasma etching: what are the ultimate limits? *Journal of Physics D: Applied Physics* **2011**, *44*, 174011.

(7) Lee, Y.; DuMont, J. W.; George, S. M. Mechanism of Thermal Al_2O_3 Atomic Layer Etching Using Sequential Reactions with $Sn(acac)_2$ and HF. *Chemistry of Materials* **2015**, *27*, 3648–3657.

(8) Lee, Y.; DuMont, J. W.; George, S. M. Trimethylaluminum as the Metal Precursor for the Atomic Layer Etching of Al_2O_3 Using Sequential, Self-Limiting Thermal Reactions. *Chemistry of Materials* **2016**, *28*, 2994–3003.

(9) Abdulagatov, A. I.; George, S. M. Thermal atomic layer etching of silicon nitride using an oxidation and "conversion etch" mechanism. *Journal of Vacuum Science & Technology A* **2020**, *38*, 022607.

(10) Zywotko, D. R.; George, S. M. Thermal Atomic Layer Etching of ZnO by a "Conversion-Etch" Mechanism Using Sequential Exposures of Hydrogen Fluoride and Trimethylaluminum. *Chemistry of Materials* **2017**, *29*, 1183–1191.

(11) DuMont, J. W.; Marquardt, A. E.; Cano, A. M.; George, S. M. Thermal Atomic Layer Etching of SiO_2 by a "Conversion-Etch" Mechanism Using Sequential Reactions of Trimethylaluminum and Hydrogen Fluoride. *ACS Applied Materials & Interfaces* **2017**, *9*, 10296–10307, PMID: 28240864.

(12) George, S. M. Mechanisms of Thermal Atomic Layer Etching. *Accounts of Chemical Research* **2020**, *53*, 1151–1160, PMID: 32476413.

(13) Lemaire, P. C.; Parsons, G. N. Thermal Selective Vapor Etching of TiO_2: Chemical Vapor Etching via WF_6 and Self-Limiting Atomic Layer Etching Using WF_6 and BCl_3. *Chemistry of Materials* **2017**, *29*, 6653–6665.

(14) Knapas, K.; Rahtu, A.; Ritala, M. Etching of Nb_2O_5 Thin Films by $NbCl_5$. *Chemical Vapor Deposition* **2009**, *15*, 269–273.

(15) Kondati Natarajan, S.; Nolan, M.; Theofanis, P.; Mokhtarzadeh, C.; Clendenning, S. B. Mechanism of Thermal Atomic Layer Etch of W Metal Using Sequential Oxidation and Chlorination: A First-Principles Study. *ACS Applied Materials & Interfaces* **2020**, *12*, 36670–36680, PMID: 32666796.

(16) van Courtland Moon, J. E. A Bridge Not Attacked: Chemical Warfare Civilian Research During World War II (review). *The Journal of Military History* **2005**, *69*, 269–269.

(17) Jia, W.-Z.; Lu, J.-Q.; Chen, P.; Wang, Y.-J.; Luo, M.-F. A novel method for the synthesis of well-crystallized β-AlF_3 with high surface area derived from γ-Al_2O_3. *J. Mater. Chem.* **2011**, *21*, 8987–8990.

(18) Chupas, P. J.; Grey, C. P. Surface modification of fluorinated aluminas: Application of solid state NMR spectroscopy to the study of acidity and surface structure. *Journal of Catalysis* **2004**, *224*, 69–79.

(19) Roodenko, K.; Halls, M. D.; Gogte, Y.; Seitz, O.; Veyan, J.-F.; Chabal, Y. J. Nature of Hydrophilic Aluminum Fluoride and Oxyaluminum Fluoride Surfaces Resulting from XeF_2 Treatment of Al and Al_2O_3. *The Journal of Physical Chemistry C* **2011**, *115*, 21351–21357.

(20) Gertsch, J. C.; Cano, A. M.; Bright, V. M.; George, S. M. SF_4 as the Fluorination Reactant for Al_2O_3 and VO_2 Thermal Atomic Layer Etching. *Chemistry of Materials* **2019**, *31*, 3624–3635.

(21) Michael, J. V.; Lim, K. P.; Kumaran, S. S.; Kiefer, J. H. Thermal decomposition of carbon tetrachloride. *Journal of Physical Chemistry* **1993**, *97*, 1914–1919.

(22) Gow, T. R.; Lin, R.; Cadwell, L. A.; Lee, F.; Backman, A. L.; Masel, R. I. Decomposition of trimethylaluminum on silicon(100). *Chemistry of Materials* **1989**, *1*, 406–411.

(23) Hill, J.; Aquino, A.; Mulcahy, C.; Harwood, N.; Jones, A.; Jones, T. The adsorption and thermal decomposition of trimethylaluminium and dimethylaluminium hydride on GaAs(100). *Surface Science* **1995**, *340*, 0–56.

(24) Squire, D. W. Mechanistic studies of the decomposition of trimethylaluminum on heated surfaces. *Journal of Vacuum Science & Technology B Microelectronics and Nanometer Structures* **1985**, *3*, 1513–1519.

(25) Pienaar, A. D. Niobium and tantalum beneficiation using gas-phase fluorination. PhD dissertation (University of Pretoria), available online: http://hdl.handle.net/2263/46243, 2015.

(26) Gosset, L.; Damlencourt, J.-F.; Renault, O.; Rouchon, D.; Holliger, P.; Ermolieff, A.; Trimaille, I.; Ganem, J.-J.; Martin, F.; Séméria, M.-N. Interface and material characterization

of thin Al_2O_3 layers deposited by ALD using TMA/H_2O. *Journal of Non-Crystalline Solids* **2002**, *303*, 1–23.

(27) Hildenbrand, D. L.; McDonald, R. A. The Heat of Vaporization and Vapor Pressure of Carbon Tetrachloride; The Entropy from Calorimetric Data. *The Journal of Physical Chemistry* **1959**, *63*, 1521–1522.

(28) Schrödinger, LLC, New York, NY, 2020, Schrödinger : Maestro suite (version 11.0). `https://www.schrodinger.com/user-announcement/announcing-schrodinger-software-release-2020-1`.

(29) Perdew, J. P.; Burke, K.; Ernzerhof, M. Generalized Gradient Approximation Made Simple. *Phys. Rev. Lett.* **1996**, *77*, 3865–3868.

(30) Garrity, K. F.; Bennett, J. W.; Rabe, K. M.; Vanderbilt, D. GBRV pseudopotential library. `https://www.physics.rutgers.edu/gbrv/`, (accessed 2020-07-25).

(31) Monkhorst, H. J.; Pack, J. D. Special points for Brillouin-zone integrations. *Phys. Rev. B* **1976**, *13*, 5188–5192.

(32) Giannozzi, P. et al. QUANTUM ESPRESSO: a modular and open-source software project for quantum simulations of materials. *Journal of Physics: Condensed Matter* **2009**, *21*, 395502 (19pp).

(33) Giannozzi, P. et al. Advanced capabilities for materials modelling with QUANTUM ESPRESSO. *Journal of Physics: Condensed Matter* **2017**, *29*, 465901.

(34) Mullins, R.; Kondati Natarajan, S.; Elliott, S. D.; Nolan, M. Self-Limiting Temperature Window for Thermal Atomic Layer Etching of HfO_2 and ZrO_2 Based on the Atomic-Scale Mechanism. *Chemistry of Materials* **2020**, *32*, 3414–3426.

(35) Arts, K.; Vandalon, V.; Puurunen, R. L.; Utriainen, M.; Gao, F.; Kessels, W. M. M. E.; Knoops, H. C. M. Sticking probabilities of H_2O and $Al(CH_3)_3$ during atomic layer deposition

of Al_2O_3 extracted from their impact on film conformality. *Journal of Vacuum Science & Technology A* **2019**, *37*, 030908.

(36) Bochevarov, A. D.; Harder, E.; Hughes, T. F.; Greenwood, J. R.; Braden, D. A.; Philipp, D. M.; Rinaldo, D.; Halls, M. D.; Zhang, J.; Friesner, R. A. Jaguar: A high-performance quantum chemistry software program with strengths in life and materials sciences. *International Journal of Quantum Chemistry 113*, 2110–2142.

(37) Young, M. J.; Bedford, N. M.; Yanguas-Gil, A.; Letourneau, S.; Coile, M.; Mandia, D. J.; Aoun, B.; Cavanagh, A. S.; George, S. M.; Elam, J. W. Probing the Atomic-Scale Structure of Amorphous Aluminum Oxide Grown by Atomic Layer Deposition. *ACS Applied Materials & Interfaces* **2020**, *12*, 22804–22814.

(38) Cano, A. M.; Marquardt, A. E.; DuMont, J. W.; George, S. M. Effect of HF Pressure on Thermal Al2O3 Atomic Layer Etch Rates and Al2O3 Fluorination. *The Journal of Physical Chemistry C* **2019**, *123*, 10346–10355.

(39) Oura, K.; Katayama, M.; Zotov, A. V.; Lifshits, V. G.; Saranin, A. A. *Surface Science: An Introduction*; Springer Berlin Heidelberg: Berlin, Heidelberg, 2003; Chapter Elementary Processes at Surfaces II. Surface Diffusion, pp 325–356.

(40) Morelock, C. R.; Hancock, J. C.; Wilkinson, A. P. Thermal expansion and phase transitions of α-AlF_3. *Journal of Solid State Chemistry* **2014**, *219*, 143 – 147.

(41) Sorrell, C.; Groetsch, J.; Soboroff, D. *Aluminum Fluxing Salts: A Critical Review of the Chemistry and Structure of Alkali Aluminum Halides*; Information circular 9069; United States Department of the Interior (Bureau of Mines), 1986; pp 1–37.

(42) Tressaud, A. *Functionalized Inorganic Fluorides: Synthesis, Characterization & Properties of Nanostructured Solids*; John Wiley and Sons, 2010; pp 173–203.

(43) Chaudhuri, S.; Chupas, P. J.; Wilson, M.; Madden, P.; Grey, C. P. Study of the Nature and Mechanism of the Rhombohedral-to-Cubic Phase Transition in α-AlF_3 with Molecular Dynamics Simulations. *The Journal of Physical Chemistry B* **2004**, *108*, 3437–3445.

(44) Zaug, J.; Stavrou, E.; Bastea, S.; Crowhurst, J.; Goncharov, A.; Roberts, S.; Plaue, J.; Carter, J.; Armstrong, M. Equations of state of anhydrous AlF_3 and AlI_3: Modeling of extreme condition halide chemistry. *The Journal of Chemical Physics* **2015**, *142*.

(45) Chen, C.; Liu, X.; Tian, B.; Shu, P.; Chen, Y.; Zhang, W.; Jiang, H.; Li, Y. Fabrication of Enhancement-Mode AlGaN/GaN MISHEMTs by Using Fluorinated Al_2O_3 as Gate Dielectrics. *IEEE Electron Device Letters* **2011**, *32*, 1373–1375.

(46) Park, B. J.; Lim, W. S.; Yeon, J. K.; Kim, Y. Y.; Kang, S. K.; Lim, J. T.; Yeom, G. Y. Fluorination of Aluminum Oxide Gate Dielectrics Using Fluorine Neutral/Ion Beams. *Journal of Nanoscience and Nanotechnology* **2011**, *11*, 5904–5908.

(47) Lee, Y.; DuMont, J. W.; George, S. M. Atomic Layer Etching of HfO_2 Using Sequential, Self-Limiting Thermal Reactions with $Sn(acac)_2$ and HF. *ECS Journal of Solid State Science and Technology* **2015**, *4*.

(48) Fischer, A.; Routzahn, A.; Lee, Y.; Lill, T.; George, S. M. Thermal etching of AlF_3 and thermal atomic layer etching of Al_2O_3. *Journal of Vacuum Science & Technology A* **2020**, *38*, 022603–(1–7).

(49) Lee, Y.; Huffman, C.; George, S. M. Selectivity in Thermal Atomic Layer Etching Using Sequential, Self-Limiting Fluorination and Ligand-Exchange Reactions. *Chemistry of Materials* **2016**, *28*, 7657–7665.

(50) Abdulagatov, A. I.; Sharma, V.; Murdzek, J. A.; Cavanagh, A. S.; George, S. M. Thermal atomic layer etching of germanium-rich SiGe using an oxidation and "conversion-etch" mechanism. *Journal of Vacuum Science & Technology A* **2021**, *39*, 022602–(1–12).

(51) Lee, Y.; George, S. M. Thermal Atomic Layer Etching of Titanium Nitride Using Sequential, Self-Limiting Reactions: Oxidation to TiO_2 and Fluorination to Volatile TiF_4. *Chemistry of Materials* **2017**, 8202–8210.

(52) Kim, J.-W.; Kim, Y.-C.; Lee, W.-J. Reactive ion etching mechanism of plasma enhanced chemically vapor deposited aluminum oxide film in CF_4/O_2 plasma. *Journal of Applied Physics* **1995**, *78*, 2045–2049.

(53) Andersson, S.; Åström, A. The Thermal Decomposition of NbO_2F. *Acta Chemica Scandinavica* **1965**, *19*, 2136–2138.

(54) Binnewies, M.; Glaum, R.; Schmidt, M.; Schmidt, P. *Chemische Transportreaktionen*; De Gruyter, 2011; pp 159–285.

(55) Schäfer, H.; Hüesker, M. Beiträge zur Chemie der Elemente Niob und Tantal. XXX. Chemische Transportreaktionen. VIII. Über die Darstellung der Nioboxide und ihren Transport im Temperaturgefälle. *Zeitschrift für anorganische und allgemeine Chemie (John Wiley and Sons)* **1962**, *317*, 321–333.

(56) Orloff, G. J.; Bernasek, S. L.; Wolk, G. L.; Coyle, R. J. Laser-Assisted Etching of Lithium Niobate. *Materials Research Society Proceedings* **1988**, *126*, 251–256.

Graphical TOC Entry